Chemistry & Biodiversity

CHEMISTRY & BIODIVERSITY

RESEARCH ARTICLE

Enhanced Bioactivity of Pyrolysis Liquid and AgNPs from *Capparis sicula* subsp. *sicula*: Chemical Characterization and Mechanistic Insights

Semiha Yenigün[1] | Yunus Basar[2] | Ibrahim Demirtas[3] | Tevfik Ozen[1] | Busran Sunyar[2] | Aybek Yiğit[4] | İlyas Yıldız[5] | Mehmet Hakkı Alma[6]

[1]Department of Chemistry, Faculty of Science, Ondokuz Mayis University, Samsun, Türkiye | [2]Research Laboratories Application and Research Center (ALUM), Iğdır University, Igdir, Turkiye | [3]Department of Pharmaceutical Chemistry, Faculty of Pharmacy, Ondokuz Mayıs University, Samsun, Turkiye | [4]Department of Pharmacy Services, Tuzluca Vocational School, Iğdır University, Igdir, Turkiye | [5]Department of Molecular Biology and Genetics, Faculty of Arts and Sciences, Tokat Gaziosmanpaşa University, Tokat, Türkiye | [6]Faculty of Forestry, Kahramanmaras Sutcu Imam University, Kahramanmaras, Türkiye

Correspondence: Ibrahim Demirtas (bdemirtas@gmail.com)

Received: 20 August 2025 | **Revised:** 12 December 2025 | **Accepted:** 17 December 2025

Keywords: *Capparis sicula* subsp. *sicula* | pyrolysis 1 | biosensor 2 | biological activity 3 | molecular docking 4 | supercritical CO_2 5

ABSTRACT

Recently, the insecticidal, antifungal, antibacterial, and antioxidant properties of pyrolysis liquid (bio-oil) obtained from agricultural and industrial plants have been investigated in foods. As no previous studies had been conducted on the *Capparis sicula* subsp. *sicula* (caper) species, this study was chosen. For the first time, a methanol–chloroform extract, pyrolysis liquid, and green-synthesized silver nanoparticles (AgNPs) were obtained from caper fruit. GC–MS/MS analysis of the extract and pyrolysis revealed linoleic and palmitic acid methyl esters. In contrast, LC–ESI–MS/MS analysis revealed high amounts of hesperidin (7.534 mg/g extract) and caffeine (0.216 mg/g extract), respectively. It was observed that the pyrolysis liquid had higher activity than the extract in terms of antioxidant activity (93.33% for DPPH and 8.01 µmol Trolox/g extract), antibacterial activity (average of 8 mm for all bacteria), and enzyme inhibition (4.72 µg/mL for α-glucosidase and 2.00 µg/mL for α-amylase). A molecular docking study found that caffeine was effective against the enzyme catalase (−6.9 kcal/mol). Therefore, by enabling the release of compounds not detected by conventional methods through pyrolysis, it will be possible to expand the use of these compounds as antioxidant and antibacterial agents in the food industry, pharmacology, and other industries.

1 | Introduction

Fruit is essential for a healthy lifestyle. Berries are often referred to as "superfruits" due to their high anthocyanin and phenol content. Phenolic compounds are a class of compounds found in all plant foods that can influence physiological processes and provide protection against chronic disease [1]. Beyond phenolics, other classes of plant bioactives, such as polysaccharides, have also garnered significant interest due to their biological activities, including anti-inflammatory effects, as demonstrated in studies on other plant species [2, 3]. While it is known that fruits are rich in bioactive compounds, there is insufficient information about the beneficial compounds in their leaves. According to studies, the phenolic compounds in the leaves are higher than those in fruits [4]. For instance, a recent study on *Kadsura coccinea* leaves revealed a rich profile of bioactive compounds with significant antioxidant and anti-inflammatory activities, underscoring the potential of leaf extracts as a source of phytochemicals [5]. Considering the known antioxidant effect of phenolic compounds, the phenolic compounds in leaves are found in greater amounts than in the fruits to exert a protective effect on the tissues in the leaves and to protect them from stress caused by sun exposure [6].

The pyrolysis process: unlike combustion, it takes place in an oxygen-free environment, and partial combustion is allowed to occur to provide the necessary heat for this process. In this process, the biomass is quickly heated to temperatures above 300°C–400°C and is turned into gaseous, liquid, and solid products [6]. During pyrolysis, the large hydrocarbon molecules in the biomass break down into smaller molecules. While fast pyrolysis produces liquid fuel, mainly known as bio-oil, slow pyrolysis produces a small number of gaseous products and solid coal. The pyrolysis process enables the conversion of waste biomass into useful liquid components [7]. The liquid fraction obtained from the pyrolysis process is referred to by various names such as bio-oil, pyrolysis oil, and pyrolysis liquid. This pyrolysis liquid is a product consisting of many oxygenated compounds such as hydroxy aldehydes, hydroxyketones, sugars, phenol derivatives, and carboxylic acids, and is estimated to contain hundreds of chemical compounds [8].

Capparis species, also known as caper plants: They grow in arid and semiarid regions and in unfavorable environments. It is a plant that can adapt to difficult climatic and soil conditions [9]. The caper plant has a very large distribution area throughout the world and is native to countries of the Middle East and the Mediterranean region. While it is found naturally distributed in almost all countries, it is cultivated in the USA, Italy, and France [10]. There are more than 250 species of capers worldwide, which belong to the Capparaceae family [11]. It is also known that *Capparis* fruit has medicinal properties such as headache, toothache, kidney disease, diuretic, constipation relief and tonic properties. It is reported in the literature that caper root, stem, and fruit extracts have anti-atherosclerotic, antihypertensive, anti-inflammatory, analgesic, antiasthmatic, antihyperlipidemic, hepatoprotective, antibacterial, antiatherosclerotic, and antifungal properties [10]. *Capparis* species are rich in glycosides, flavonoids, polyphenols, phenolic acids, terpenoids, saponins, sterols, and tannins [12]. In this context, comparing and evaluating the biological activity of a pyrolysis sample of *C. sicula*, a plant known for its numerous beneficial properties, with a sample obtained through traditional extraction methods, could facilitate its further utilization in various applications

This study aimed to determine, for the first time, the methanol–chloroform extract, pyrolysis liquid and AgNPs obtained from *Capparis sicula* subsp. *sicula* (CSS). The phytochemical properties (GC–MS/MS, LC–ESI–MS/MS, NMR), biological activities (antioxidant, enzyme inhibition and antibacterial) and characteristic properties (UV–Vis, Fourier transform infrared [FT-IR], x-ray diffraction [XRD], transmission electron microscopy [TEM], and field-emission scanning electron microscopy [FE-SEM]) of the samples were investigated. For this purpose, the antioxidant and total phenolic contents of the extract and pyrolysis liquid were determined using the biosensor method for the first time. The chemical profiling results were directly linked to the observed biological activities to provide clearer interpretation. The interactions of the major components detected by LC–ESI–MS/MS in both the extract and the pyrolysis liquid with antioxidant and antibacterial enzymes were theoretically calculated using in silico methods. This finding allows a more coherent flow from compound identification to functional outcomes, emphasizing the relationship between chemical composition and biological performance. In this way, the phytochemical and biological activities of CSS samples obtained by different methods were compared. It is believed that this study may provide valuable indications for potential applications in various fields.

2 | Results and Discussion

Establishing the physicochemical properties of the materials, particularly the biosynthesized AgNPs, is essential for correctly interpreting their subsequent antioxidant, enzyme inhibitory, and antibacterial behaviors. Since nanoparticle size, morphology, and surface chemistry directly influence bioactivity, the characterization data serve as the scientific foundation for the results discussed in later subsections.

2.1 | Characterization of AgNPs

Nanotechnology is a branch of science that offers different perspectives on other scientific disciplines working at the nanoscale, including bioengineering, food technology, dentistry, and pharmacy [13]. Many techniques are used to create nanomaterials, which have numerous applications. Green synthesis is one of these techniques for nanoparticle production. Green synthesis method is critical to the development of nanomaterials in the future. It is commonly acknowledged in nanotechnology that this area of nanoscience is important for creating safe and eco-friendly nanoparticles [14]. In green synthesis, plant extract is used to synthesize metal-based nanoparticles. Numerous recent studies have demonstrated the potential role of plant extracts in the non-hazardous production of nanomaterials. Greener nanoparticles, including cobalt, copper, silver, gold, palladium, platinum, zinc oxide, and magnetite, are successfully synthesized from plants [15]. Over the last decade, a diverse range of biological systems has been synthesized inorganic metal ions into reductively active proteins and metabolites, including human cells, bacteria [16], fungi [17], and plants and algae [18]. Its ability enables it to convert metal into nanoparticles. The unique optical [19] and chemical properties of metallic nanoparticles have drawn a lot of attention to their fabrication using biological structures [20]. Extracts from various plants and fruits are utilized in the synthesis of nanoparticles through a nature-friendly green synthesis process. In this study, we determined the characteristic properties of the AgNP obtained from CSS fruit.

2.2 | UV–Vis Spectroscopy

UV–Vis absorbance spectroscopy (Figure 1a) was used for the first step of characterization. UV–Vis spectroscopy is a widely used analytical technique for verifying the formation of metal nanoparticles and analyzing their optical properties. It is especially crucial for characterizing silver nanoparticles (AgNPs) due to the detection of the surface plasmon resonance (SPR) band. For UV–Vis analysis in this study, an Agilent Cary 60 UV–Vis device was used [21]. The peak observed at around 228 nm is associated with the $\pi \rightarrow \pi^*$ characteristic transitions of phenolic compounds, flavonoids, and other organic molecules found in plant extracts. Similarly, the peak around 276 nm reflects $n \rightarrow \pi^*$ transitions of phenolic compounds, indicating the presence of aromatic structures in the extract. Conversely, the broad band

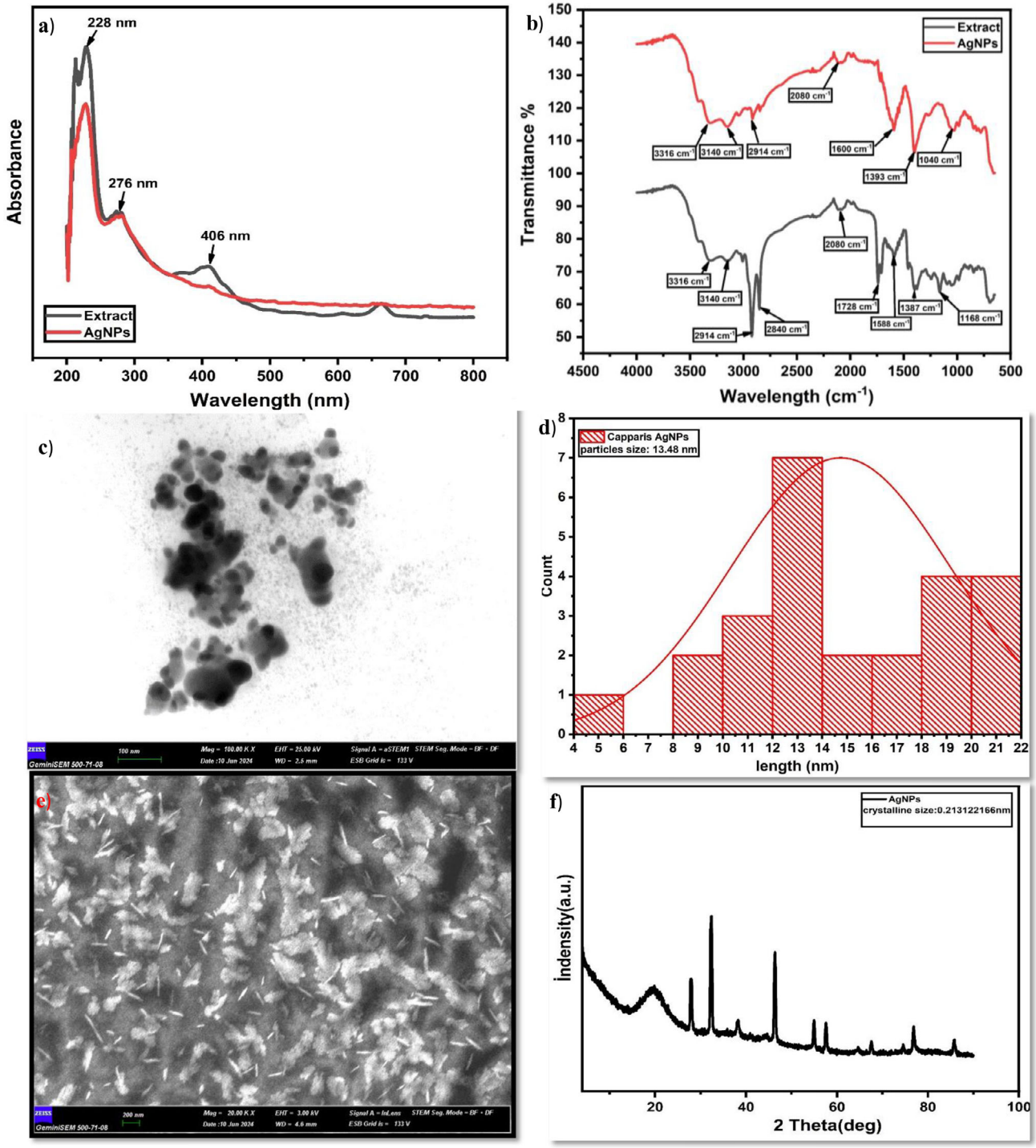

FIGURE 1 | Characteristic properties of CSS AgNPs: (a) UV–Vis, (b) FT-IR, (c) TEM, (d) TEM histogram, (e) FE-SEM, and (f) XRD image.

appearing around 406 nm is the typical SPR peak of AgNPs. The SPR peak for AgNPs is generally reported to occur within the 380–450 nm range. Therefore, the peak at 406 nm suggests that the particles are likely to be spherical or semi-spherical [22, 23].

2.3 | FT-IR Spectroscopy

One of the simplest and most popular characterization methods for identifying the functional groups on the surface of biosynthetically produced AgNPs and revealing the chemical interactions between the plant extract and the nanoparticles is FT-IR spectroscopy [24]. An Agilent Cary 630 FT-IR device was used in these analyses. Significant peak shifts and intensity changes between the FT-IR spectra of the plant extract and AgNPs show that the extract compounds actively contribute to the reduction of silver ions and the stabilization of the formed nanoparticles. The —OH and —NH stretching in phenolic chemicals and protein-like structures is represented by the wide bands seen in the extract between 3316 and 3140 cm^{-1}. These functional groups

may be involved in the reduction process, as indicated by the weakening of these bands in the AgNP spectra. In addition, the adsorption of aliphatic and nitrile/alkyne compounds to the nanoparticle surface is supported by the changes seen in the aliphatic C—H stretching between 2914–2840 cm^{-1} and the C≡C/C≡N bands at 2080 cm^{-1}. Carbonyl-containing phenolic or organic acid derivatives interact with Ag^{+} ions and experience structural changes, as seen by the shift of the carbonyl (C═O) band, which was prominent at 1728 cm^{-1} in the extract, to about 1600 cm^{-1} in AgNPs. In addition, polysaccharides and phenolic compounds function as stabilizers on the nanoparticle surface, as demonstrated by the C—N/C—H bands in the 1393–1387 cm^{-1} region and the variations in the C—O and C—O—C stretches in the 1168–1040 cm^{-1} range [25–27]. Overall, these findings confirm the successful biosynthesis of AgNPs by the functional groups in the plant extract, which act as both reducing agents and stabilizers.

2.4 | TEM

A ZEISS GeminiSEM type scanning electron microscope was used for STEM studies. The physical and chemical properties of nanoparticles vary depending on their size and shape. As a result, consistent nanoparticle creation techniques are employed. A good analytical tool for seeing the size and form of nanoparticles is a TEM apparatus. TEM pictures show that a variety of forms, including square, rectangular, semi-spherical, and spherical, are present. On the other hand, TEM images showed that most 25-AgNPs were between 4 and 22 nm in size, with an average size of 13.48 ± 4.40 nm (min–max, 4.632–21.578) [28] (Figure 1c,d).

2.5 | FE-SEM and FE-SEM–EDX

The FE-SEM device was used to study the morphology of AgNPs (Figure 1e). The ZEİSS GeminiSEM model device was used. A small number of oval AgNPs are also seen; however, the majority of the particles are spherical. In addition, additional examination of the silver particles using energy dispersive spectroscopy verified the existence of the elemental silver signal's existence. The EDAX images of the artificial AgNPs are displayed in Figure S1 and Table S1 [15].

2.6 | XRD

XRD is used to characterize the nanoparticles manufactured using this process. This technique confirms the silver content of the particles and provides structural information about them. A Malvern Panalytical Empyrean model x-ray diffractometer (Malvern Panalytical, Malvern, UK) was used to conduct XRD investigations. The analyses were conducted at a tube voltage of 45 kV using Cu Kα radiation (λ = 1.5406 Å). The step size was set at 4°, and measurements were taken in the 2θ range of 0°–100°. The XRD analysis pattern of the AgNPs is displayed in Figure 1f. Diffraction peaks were seen in the pattern at points 19.95°, 27.56°, 32.84°, 37.88°, 46.02°, 54.64°, 58.02°, 63.35°, 76.51°, and 85.44°, in that order. AgNPs may be linked to these diffraction peaks (32.84° and 46.81°) [29]. Nonetheless, the presence of bioorganic molecules clustered around silver can explain the weak diffraction peaks at these locations. Also, the average crystalline size of the AgNPs was estimated using (Equation 1), the Debye–Scherrer's equation [30]:

$$D\% = \%0.9\lambda/\beta\cos\theta \quad (1)$$

According to the Debye–Scherrer equation, the average crystal size was determined as 0.213 nm.

2.7 | GC–MS/MS, LC–ESI–MS/MS, and NMR Results

Fatty acid and volatile oil contents of hexane, methanol–chloroform extract, and pyrolysis liquid of CSS fruit were analyzed by GC–MS/MS (Figure S2 and Table 1). Accordingly, in the hexane extract; Linoleic acid methyl ester (56.46%), oleic acid methyl ester (25.86%), palmitic acid methyl ester (12.95%), in methanol–chloroform extract; linoleic acid methyl ester (40.46%), palmitic acid methyl ester (29.29%), oleic acid methyl ester (11.84%), and pyrolysis liquid; The compounds palmitic acid methyl ester (37.64%), linoleic acid methyl ester (29.18%), oleic acid methyl ester (12.29%), were detected in the highest amount. Thus, the main components were determined to be palmitic acid methyl ester, linoleic acid methyl ester, and oleic acid methyl ester.

Phenolic content analysis of the methanol–chloroform extract of caper fruit and pyrolysis liquid was performed by LC–ESI–MS/MS (Figure S3 and Table 2). Accordingly, in the methanol–chloroform extract; hesperidin (7.534 mg/g extract), rutin (2.830 mg/g extract), vanillic acid (0.420 mg/g extract), and pyrolysis liquid; caffeine (0.216 mg/g extract), rutin (0.039 mg/g extract), *o*-coumaric acid (0.017 mg/g extract) were determined in the highest amount. In a similar study, a content analysis of CSS methanol extract by HPLC identified and isolated glucoraphanin and rutin as the major components [31]. According to the results, CSS was found to be rich in rutin.

The ^{1}H NMR of the extract shows the presence of olefinic protons at δ 4.31 (dd, J = 11.8, 4.3 Hz, 1H), 4.22–4.12 (m, 1H) ppm, respectively. The rest of the spectrum signals characteristic of a long chain fatty acid or ester bearing a long chain of about 23 internal CH_2, 1 CH, 8 terminal or branched CH_2, and 3 terminal CH_3 as shown on the summary of spectra data (Figure 2).

^{1}H NMR (400 MHz, $CDCl_3$) δ 5.37 (dt, J = 7.4, 3.6 Hz, 7H), 4.31 (dd, J = 11.8, 4.3 Hz, 1H), 4.22–4.12 (m, 1H), 3.68 (s, 1H), 2.79 (t, J = 6.5 Hz, 2H), 2.41–2.28 (m, 5H), 2.05 (dd, J = 14.9, 7.1 Hz, 8H), 1.64 (d, J = 7.3 Hz, 4H), 1.29 (d, J = 18.8 Hz, 47H), 0.89 (dd, J = 7.0, 3.9 Hz, 9H).

The ^{1}H NMR of the pyrolyzed sample is very similar to that of the extract; we noticed the disappearance of the signals at δ 4.34 and 4.16 ppm, indicating the absence of olefinic protons. The rest of the spectrum is identical, but we noticed a reduction in the number of CH_2, group indicating the molecule lost some CH_2 during the pyrolysis (from 48 H to 30 H), which may have resulted from some kind of rearrangement during pyrolysis (Figure 2).

TABLE 1 | The extract and the pyrolysis liquid of CSS content analysis by GC–MS/MS.

No.	RT (min)	Compound name	Extract (H), %	Extract (MC), %	Pyrolysis, %
1	42.12	Myristic acid, methyl ester	0.19	0.96	0.83
2	46.91	Palmitoleic acid, methyl ester	0.04	0.81	—
3	47.44	Palmitic acid, methyl ester	12.95	29.29	37.64
4	49.18	Hexadecanoic acid, 15-methyl-, methyl ester	0.04	—	—
5	49.85	Heptadecanoic acid, methyl ester	0.02	—	—
6	50.73	*cis*-10-Heptadecenoic acid	0.04	—	—
7	51.45	Linoleic acid, methyl ester	56.46	40.46	29.18
8	51.59	Oleic acid, methyl ester	25.86	11.84	12.29
9	51.71	Oleic acid, methyl ester-isomer	1.83	7.31	6.94
10	52.15	Stearic acid, methyl ester	0.46	6.8	9.20
11	53.22	Undetermined	0.07		
12	53.62	8,11-Octadecadienoic acid, methyl ester	—	—	1.34
13	56.06	Undetermined	0.07		
14	56.21	Undetermined	0.21		
15	57.00	11-Eicosenoic acid, methyl ester	0.85	—	—
16	57.00	*cis*-11-Eicosenoic acid	0.83	0.09	—
17	57.92	Arachidic acid methyl ester	—	1.11	1.05
18	65.25	Methyl 11-docosenoate	0.55	—	—
19	66.18	Behenic acid, methyl ester	0.18	1.23	1.18
20	71.99	Lignoceric acid methyl ester	—	0.09	0.15
21	74.22	Squalene	—	—	0.20

Abbreviations: H, hexane; MC, methanol–chloroform; RT, retention time.

TABLE 2 | The extract and the pyrolysis of CSS content analysis by LC–ESI–MS/MS.

No.	RT (min)	Compound	Extract (mg/g extract)	Pyrolysis (mg/g extract)
1	8.946	Chlorogenic acid	0.004	—
2	9.695	Caffeine	—	0.216
3	11.370	Vanillic acid	0.420	—
4	10.058	Caffeic acid	0.015	—
5	10.431	Hydroxybenzaldehyde	0.048	0.002
6	10.856	Vanillin	0.013	0.009
7	12.078	Rutin	2.830	0.039
8	12.618	*trans*-Ferulic acid	0.028	—
9	11.484	*o*-Coumaric acid	0.015	0.017
10	11.517	Taxifolin	0.009	0.007
11	12.367	Salicylic acid	0.030	—
12	12.116	Isoquercitrin	0.124	0.040
13	12.078	Hesperidin	7.534	0.073
14	13.721	*trans*-Cinnamic acid	0.014	—
15	14.811	Chrysin	0.006	—

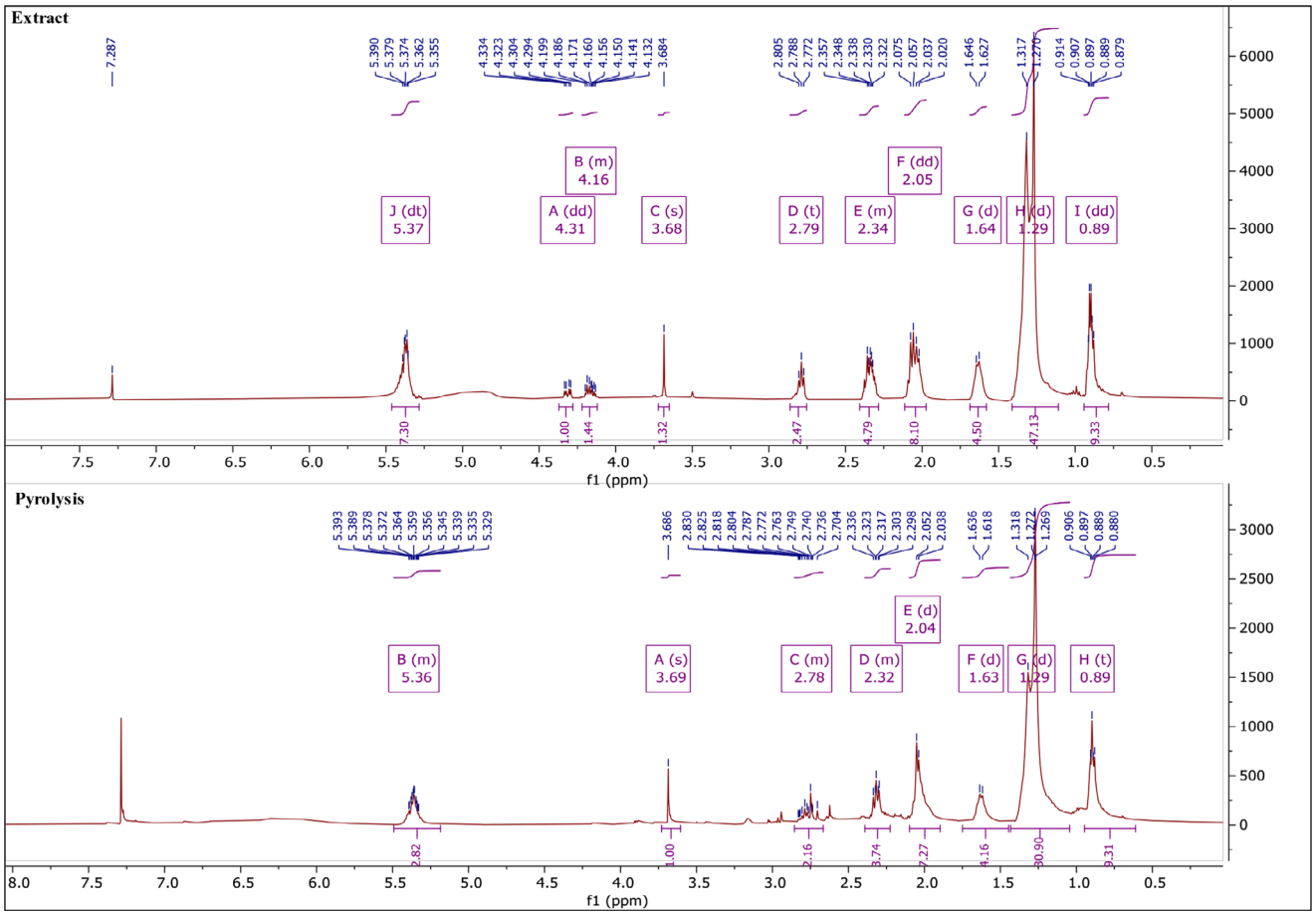

FIGURE 2 | ^{1}H NMR spectrum of the extract and pyrolysis of CSS.

^{1}H NMR (400 MHz, $CDCl_3$) δ 5.49–5.18 (m, 3H), 3.69 (s, 1H), 2.86–2.67 (m, 2H), 2.39–2.23 (m, 4H), 2.04 (d, J = 5.6 Hz, 7H), 1.63 (d, J = 7.4 Hz, 4H), 1.29 (d, J = 18.4 Hz, 31H), 0.89 (t, J = 5.3 Hz, 9H).

2.8 | Antioxidant Activity and Total Phenolic Content

The antioxidant activity tests were performed using new methods presented in the literature. These tests were performed as the DPPH˙ scavenging test, the Folin–Ciocâlteu reagent (FCR) total phenol test, and the ferric reducing power assay (FRAP) test. This method is based on a different principle than the UV spectrometer used in literature. This method measures the potential difference. In this way, it can be applied to all samples whose color is not cloudy or turbid. The name of this method is the potentiometric test of antioxidant activity. In this method, three different electrodes have been developed and used for three different tests. DPPH-SPMB for the DPPH˙ test. The preparation of the electrode was reported in our previous study [32]. More details about the FCR total phenol biosensor FCR-SPMB and FRAP-TEA are given in another publication [33].

If we analyze the results, we see that the best result for the DPPH˙ scavenger was obtained for the pyrolysis sample (93.33%). We also see that the pyrolysis sample is more active than the 12.5 ppm (60.33%) and 25 ppm (85.23%) Trolox standards we used. When we compare the methanol–chloroform extract of capers (71.67%) with the standards, we see that it has moderate free radical scavenging activity.

In the FRAP, we see that the pyrolysis sample (8.01 µmol Trolox/g extract) is four times more active than the methanol–chloroform extract (2.22 µmol Trolox/g extract) and the 12.5 ppm (1.81 µmol Trolox/g extract). At 25 ppm (2.82 µmol Trolox/g extract) it was more than twice as active as the Trolox standard.

When examining the total phenolic content of FCR, we observe conflicting results in the FRAP and DPPH˙ tests. The methanol–chloroform extract (222.368 g gallic acid (GA)/extract) was more active than the pyrolysis sample (160.25 g GA/extract). The higher total phenolic content in the extract than in the pyrolysis test supports the LC–MS/MS results. A total of 14 different compounds were identified in the LC–MS/MS analysis of the extract, while only eight were identified in the pyrolysis test. As can be understood from these results, it can be assumed that phenolic compounds may have transformed into other components during the pyrolysis process, and this was confirmed by the NMR results. In the FCR method, results were determined using GA, while in the other two antioxidant activity methods, results were determined using Trolox. Therefore, considering the structures of both compounds, it is thought that the components affecting the results in the extract and pyrolysis are similar to those of these two compounds or that the compounds converted

TABLE 3 | The antioxidant activities from the extract and the pyrolysis of CSS.

Samples/standards	DPPH˙, %	FRAP (μmol Trolox/g extract)	FCR (g GA/g extract)
Extract	71.67 ± 0.035[c]	2.22 ± 0.333[bc]	222.36 ± 0.015[b]
Pyrolysis	93.33 ± 0.039[a]	8.01 ± 0.435[a]	160.25 ± 0.018[c]
100 ppm Trolox	99.44 ± 0.020[a]	—	—
50 ppm Trolox	96.67 ± 0.019[a]	—	—
25 ppm Trolox	85.25 ± 0.023[b]	2.82 ± 0.483[b]	400.23 ± 0.025[a]
12.5 ppm Trolox	60.67 ± 0.025[d]	1.80 ± 0.735[c]	222.23 ± 0.045[b]

Note: $n = 3$, $p < 0.05$. Expressions such as a, b, c express statistical significance (one-way ANOVA Tukey HSD test).

TABLE 4 | The enzyme inhibition from the extract and the pyrolysis of CSS.

Samples/standards	XO inhibition (IC_{50}, μg/mL)	α-Glucosidase inhibition (IC_{50}, μg/mL)	α-Amylase inhibition (IC_{50}, μg/mL)
Extract	3.92 ± 0.06[a]	10.27 ± 1.51[b]	4.50 ± 2.20[b]
Pyrolysis	—	4.72 ± 0.10[a]	2.00 ± 0.25[a]
Allopurinol	19.95 ± 1.41[b]	—	—
Acarbose	—	75.98 ± 1.69[c]	17.87 ± 0.25[c]

Note: $n = 3$, $p < 0.05$. Expressions such as a, b, c express statistical significance (one-way ANOVA Tukey HSD test).

to these compounds influence activity. In other words, we see that the pyrolysis process activates the compounds in the DPPH˙ scavenging test and the FRAP reduction test, while reducing the total phenolic content (Table 3).

Antioxidant studies indicate that the pyrolysis liquid exhibits higher activity than the extract. We assume this is due to the higher amounts of caffeine and palmitic acid in the pyrolysis compared to other compounds in the pyrolysis and in the extract. Therefore, the isolation and use of valuable compounds in the pyrolysis technique can be widely used as antioxidants.

2.9 | Enzyme Inhibitions

Xanthine oxidase (XO) is an enzyme that plays a crucial role in the conversion of hypoxanthine to xanthine during the urea cycle. If excessive xanthine accumulation occurs in the body, it can lead to various diseases, particularly gout. Therefore, this enzyme must be inhibited to prevent xanthine accumulation. For this reason, many drugs currently available on the market are used to inhibit this enzyme. However, many side effects are observed in these drugs. For this reason, research on the use of drugs obtained from natural products is increasing day by day. In our study, we investigated whether caper can be a XO inhibitor [34]. As can be seen from the results in Table 4, while no inhibitory effect of pyrolysis was observed, an inhibitory effect was observed in the methanol:chloroform extract. In fact, this effect (3.92 ± 0.06 μg/mL for extract) was higher than the drug (19.95 ± 1.41 μg/mL for allopurinol).

A major global public health concern, diabetes mellitus (DM) is a chronic metabolic disease that contributes significantly to morbidity and death worldwide. DM and its related complications have a significant impact on human quality of life and have emerged as a significant public health issue. Without altering insulin resistance, current antidiabetic medications either enhance insulin production or change the way glucose is absorbed and excreted [35]. The primary pancreatic digestive enzyme is amylase, which is reliant on calcium. Maltodextrins, glycogen, amylose, and amylopectin are among the carbohydrates that have 1,4-glycosidic linkages that it cleaves. This enzyme mostly breaks down starch in humans. The intestinal epithelium secretes mammalian α-glucosidase, which is the main catalyst for breaking down polysaccharides into absorbable monosaccharides. These brush boundary α-glucosidase enzymes include lactase, sucrase-isomaltase, and maltase-glucoamylase [36]. Remarkably, blocking α-glucosidases has emerged as a key tactic in the management of DM. By converting 1,4-alpha links to glucose, the digestive enzyme α-glucosidase, also known as maltase, catalyzes the breakdown of carbohydrates [37]. As can be seen in Table 4, pyrolysis was shown to inhibit α-amylase and α-glucosidase more than extract and acarbose. The high antidiabetic effect of the pyrolysis liquid may be due to its caffeine and palmitic acid content. Conversely, the extract contains no caffeine, instead containing high amounts of hesperidin. It also contains high amounts of linoleic acid instead of palmitic acid.

2.10 | Antibacterial Activity

As various medically and economically important organisms develop resistance to existing pesticides and antimicrobials, new products with biocidal potential have been sought to combat these organisms. AgNPs have shown significant antibacterial activity against a variety of Gram-positive and Gram-negative

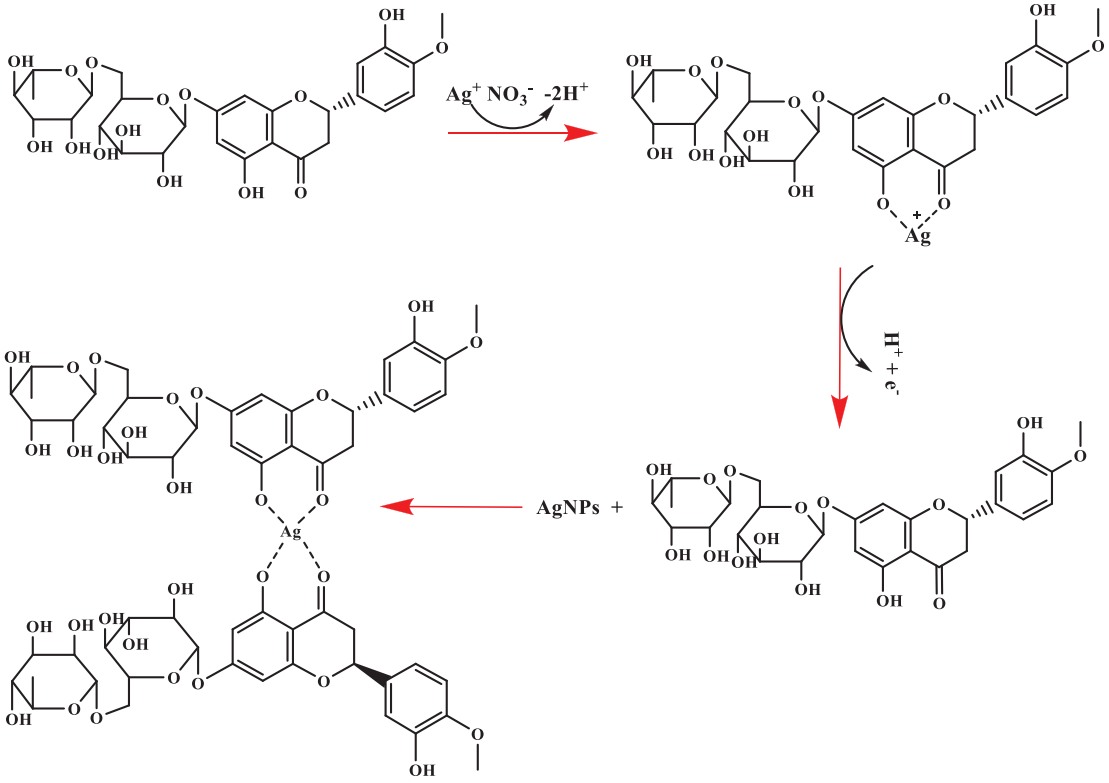

FIGURE 3 | Possible AgNP-hesperidin mechanism.

bacteria [38]. However, the exact process by which they exhibit bactericidal or growth-inhibitory properties is still unclear [39].

The literature currently describes three different ways in which AgNPs achieve their antibacterial activity [40], which can be influenced by their stability and aggregation state [41]. Beyond their direct antibacterial effects, AgNPs are also widely employed in biosensing platforms for bacterial detection due to their unique optical properties and surface functionalization capabilities [42]. The first assumption is that AgNPs act at the membrane level because they can pass through the outer membrane, accumulate in the inner membrane, and adhere to cells, which can lead to damage and instability, increase membrane permeability, cause leakage of cell contents, and ultimately lead to cell death [43]. According to the second mechanism, AgNPs can enter the cell and interact with phosphorus or sulfur groups located in intracellular materials such as DNA and proteins to alter their structure and function. They can also break through the cell membrane and alter its permeability and structure. They can also interact with the thiol groups in enzymes, generate free radicals and reactive oxygen species (ROS), alter the respiratory chain of the inner membrane, damage the intracellular machinery, and induce the apoptotic process. The release of silver ions from nanoparticles, which, due to their size and charge, can interact with cellular components and alter metabolic pathways, membranes, and even genetic material, is the third proposed mechanism, concurrent with the other two [44]. In the LC–ESI–MS/MS analysis of the extract from the nanoparticles, hesperidin was determined to be the main component. Considering the complex mechanism that various metals form with hesperidin, the mechanism which Ag and hesperidin can form in this study is shown in Figure 3.

The antibacterial properties of the caper plant extract, pyrolysis liquid, and AgNP samples were determined using the disk diffusion method (Figure 4). According to the results, it was found that the extract of the caper plant showed no antibacterial activity against *Escherichia coli*, *Pseudomonas aeruginosa*, and *Klebsiella pneumoniae* strains at all concentrations. However, a 9 mm zone was detected against *Staphylococcus aureus* at a concentration of 40 mg/mL. It was found that AgNPs with green synthesis showed antibacterial activity against *E. coli*, *K. pneumoniae*, *P. aeruginosa*, and *S. aureus* strains. While *S. aureus*, *E. coli*, *P. aeruginosa*, and *K. pneumoniae* each showed activity at the highest dose of 80 mg/mL, a decrease in zone diameter was observed as the concentration decreased. At the highest concentration (80 mg/mL), the zone diameter was 16 mm against the largest *S. aureus*, while at the lowest concentration (10 mg/mL), a zone diameter of 9 mm was observed against *P. aeruginosa*. The antibacterial activity of the caper pyrolysis liquid was also tested. Although the results varied, the highest zone diameter was observed at a concentration of 80 mg/mL against *P. aeruginosa*, while the lowest zone diameter was observed at concentrations of 20 and 10 mg/mL against *S. aureus*. The zone diameter of the antibiotic disks used, gentamicin (10 µg), was 18 mm for *E. coli*, 18 mm for *P. aeruginosa*, 18 mm for *K. pneumoniae*, and 23 mm for *S. aureus*; amoxicillin (25 µg) has a zone diameter of 20 mm for *E. coli*, 26 mm for *P. aeruginosa*, and 24 mm for *S. aureus*. Tetracycline (30 µg) was found to have zone diameters of 23 mm for *E. coli*, 27 mm for *P. aeruginosa*, 12 mm for *K. pneumoniae*, and 17 mm for *S. aureus*. The dimensions (mm) of the zones of inhibition of the disks with caper extract, pyrolysis liquid, and AgNPs from green synthesis, as well as antibiotics, against the test microorganisms at different concentrations, are shown in Table 5.

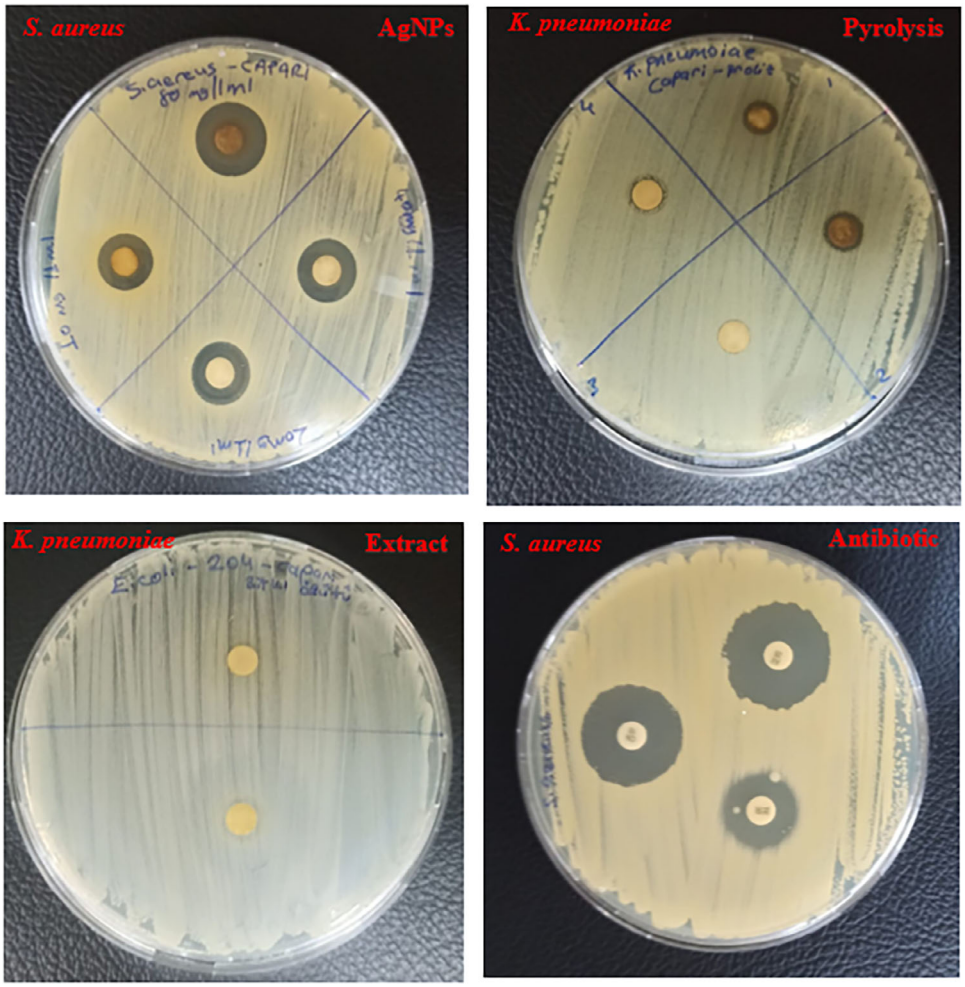

FIGURE 4 | The inhibition zones for antibacterial activity of the AgNPs, the pyrolysis, and the extract of CSS.

TABLE 5 | The antibacterial activity result of the extract, the AgNPs and the pyrolysis from CSS (mm).

Samples/antibiotic	Concentration	*Escherichia coli*	*Klebsiella pneumoniae*	*Pseudomonas aeruginosa*	*Staphylococcus aureus*
Extract	10 mg/mL	—	—	—	—
	20 mg/mL	—	—	—	—
	40 mg/mL	—	—	—	9
	80 mg/mL	—	—	—	—
AgNPs	10 mg/mL	11	10	9	13
	20 mg/mL	11	12	11	14
	40 mg/mL	13	13	14	14
	80 mg/mL	14	13	14	16
Pyrolysis	10 mg/mL	8	8	7	7
	20 mg/mL	8	—	8	7
	40 mg/mL	8	8	9	8
	80 mg/mL	9	8	11	9
Antibiotic	CN	18	18	18	23
	AX	20	—	26	24
	TE	23	12	27	17

Abbreviations: AX, amoxicillin (25 μg); TE, tetracycline (30 μg); CN, gentamicin (10 μg).

In pyrolysis, the compounds found can be associated with active compounds such as phenols, alcohols, acids, aldehydes, alkanes, benzenes, furans, and naphthalene. For example, phenolic compounds found in plants have been linked to the antibacterial activity of plant extracts, which disrupts selective permeability and enzyme inactivation through their interaction with cell walls and membranes [45]. Quinones have been linked to cell wall disruption, enzyme inactivation, and may also render substrates unavailable to microorganisms [46]. This information provides insight into how the composition of pyrolysis can exert antibacterial activity.

Our study showed that the caper extract was only effective against the *S. aureus* strain, but exhibited no activity against the *E. coli*, *P. aeruginosa*, and *K. pneumoniae* strains. The antibacterial activity of AgNP and pyrolysis liquid varied depending on the microorganisms tested, such as *S. aureus*, *E. coli*, *P. aeruginosa*, and *K. pneumoniae*, but proved to be effective against all of them. AgNP, it was found that the zone diameters of all strains used were close to each other, and the highest activity belonged to the *S. aureus* strain. The highest activity in the pyrolysis liquid was observed against *P. aeruginosa* bacteria. Benakashani et al. tested the antibacterial activity using the disk diffusion method using nanoparticles (AgNPs) with the aqueous extract of *C. spinosa* leaves [47]. As a result of the study, it was found that the extract of the caper plant showed no activity against the strains *E. coli*, *S. typhimurium*, *S. aureus*, and *B. cereus*, while the AgNPs from green synthesis showed activity against all strains. Javadian et al. tested the plant extract of *C. spinosa* and AgNPs with green synthesis against the microorganisms *S. pyogenes*, *S. pneumoniae*, *S. saprophyticus*, *H. alvei*, *Ac. baumannii*, *E. faecalis*, *P. mirabilis*, *S. marcescens*, and *S. aureus*, and showed activity [48]. Salmen et al. found that the AgNPs of the plant *C. spinosa* had antibacterial activity against *S. aureus*, *S. epidermidis*, MRSA and *E. coli* strains, with a zone diameter of 7–13 mm [49]. Therefore, the results we obtained are consistent with studies in literature.

It is known that silver has an antibacterial effect even at low concentrations [50]. However, the pyrolysis liquid contains phenolic compounds, fatty acids, and acetic acid as well as organic oils. Studies have shown that the antimicrobial properties of bio-oils are due to these rich compounds [8]. Therefore, the high antibacterial properties of the pyrolysis liquid in our study are due to its high content.

2.11 | In Silico Studies

Appropriate experimental techniques or computational methods are widely used in drug design. While some drug developers prefer alternative experimental solutions, others use computerized methods that are cost-effective and informative. Molecular modeling methods can be used not only to support experimental studies, but also to predict the results obtained in a simulation environment. Docking is a method to study the binding of two molecules in their stable conformations. Molecular docking shows how molecules interact with enzymes. To create a lattice box in molecular docking, the active site must be determined [51]. Which pose of the molecule and the enzyme is used most effectively is determined by the MolDock score. Molecular dynamics (MD) simulations are a method for improving molecular docking procedures. The MD, from fast internal movements to slow conformational changes, the dynamic behavior of proteins at different time periods can be observed in protein folding processes. In the biomolecular system, it can determine the effect of molecules on protein structure and stability to determine various thermodynamic parameters, such as density, conductivity, dipolar moment, interaction energies, and entropies [52].

2.12 | Molecular Docking Results

The molecular interaction profiles were interpreted in relation to the observed biological activities by evaluating the docking results in terms of hydrogen bonding, hydrophobic contacts, and electrostatic interactions for each enzyme. These interaction patterns, particularly the strong binding affinity of caffeine toward catalase, provide mechanistic support for the experimentally observed antioxidant and enzyme inhibitory effects, as follows. It was observed that caffeine formed five hydrogen bonds and eight hydrophobic interactions with glutathione reductase; eight hydrogen bonds and six hydrophobic interactions with glutathione oxidase; four hydrogen bonds, two electrostatic interactions, and eight hydrophobic interactions with catalase; nine hydrogen bonds, other interaction, and eight hydrophobic interactions with SOD; one hydrogen bond and four hydrophobic interactions in its interaction with the DD-peptidase. The hydrogen bonds are the carbon-hydrogen bonds (TRP6, SER279, ASP96, PRO92) for glutathione reductase; the conventional (SER321) and carbon-hydrogen bonds (SER321, GLN307, ARG297, ASN320, GLU294) for glutathione oxidase; the conventional (HIS175) and carbon–hydrogen bonds (ASN403, ASN324, PRO172) for catalase; the conventional (VAL148) and carbon–hydrogen bonds (GLY147, VAL148, VAL7, CYS146) for SOD; the conventional hydrogen bond (ASN161) for DD-peptidase. Pi–sigma (SER279), alkyl (VAL278, ILE283, PRO92) and pi–alkyl (PHE95, PRO92, VAL278) interactions are seen in hydrophobic interactions for glutathione reductase; alkyl (ILE298, ARG296) and pi–alkyl (ARG296, ILE298) interactions are seen in hydrophobic interactions for glutathione oxidase; pi–sigma (HIS166), pi–pi T-shaped (HIS166), alkyl (ARG170, ARG388, PRO172) and pi–alkyl (HIS175, PRO172, ARG388) interactions are seen in hydrophobic interactions and electrostatic interactions (ASP389) for catalase; alkyl (VAL148, VAL7) and pi–alkyl (VAL148, VAL7) interactions are seen in hydrophobic interactions and pi–sulfur interaction (CYS56) for SOD; pi–pi T-shaped (TRP233) and pi–alkyl (PHE120, TRP233) interactions are seen in hydrophobic interactions for DD-peptidase. While these interactions are visually shown in Figure 5, bond distances, categories, and the amino acids with which they interact are presented in Tables S2–S6. The binding energy of caffeine with glutathione reductase, glutathione oxidase, catalase, SOD, and DD-peptidase was determined to be −4.7, −6.3, −6.9, −4.7, and −4.8, respectively. According to the docking results, the caffeine compound was found to be an inhibitor of the enzyme catalase.

Catalase is an enzyme that is needed to neutralize harmful hydrogen peroxide. Catalase is involved in the second stage of defense against ROS [53]. The catalase reaction takes place in two steps. Under certain conditions, catalase can act as a peroxidase, that is, it uses H_2O_2 to oxidize secondary two-electron and one-electron donors. In the latter case, the catalase is reduced to

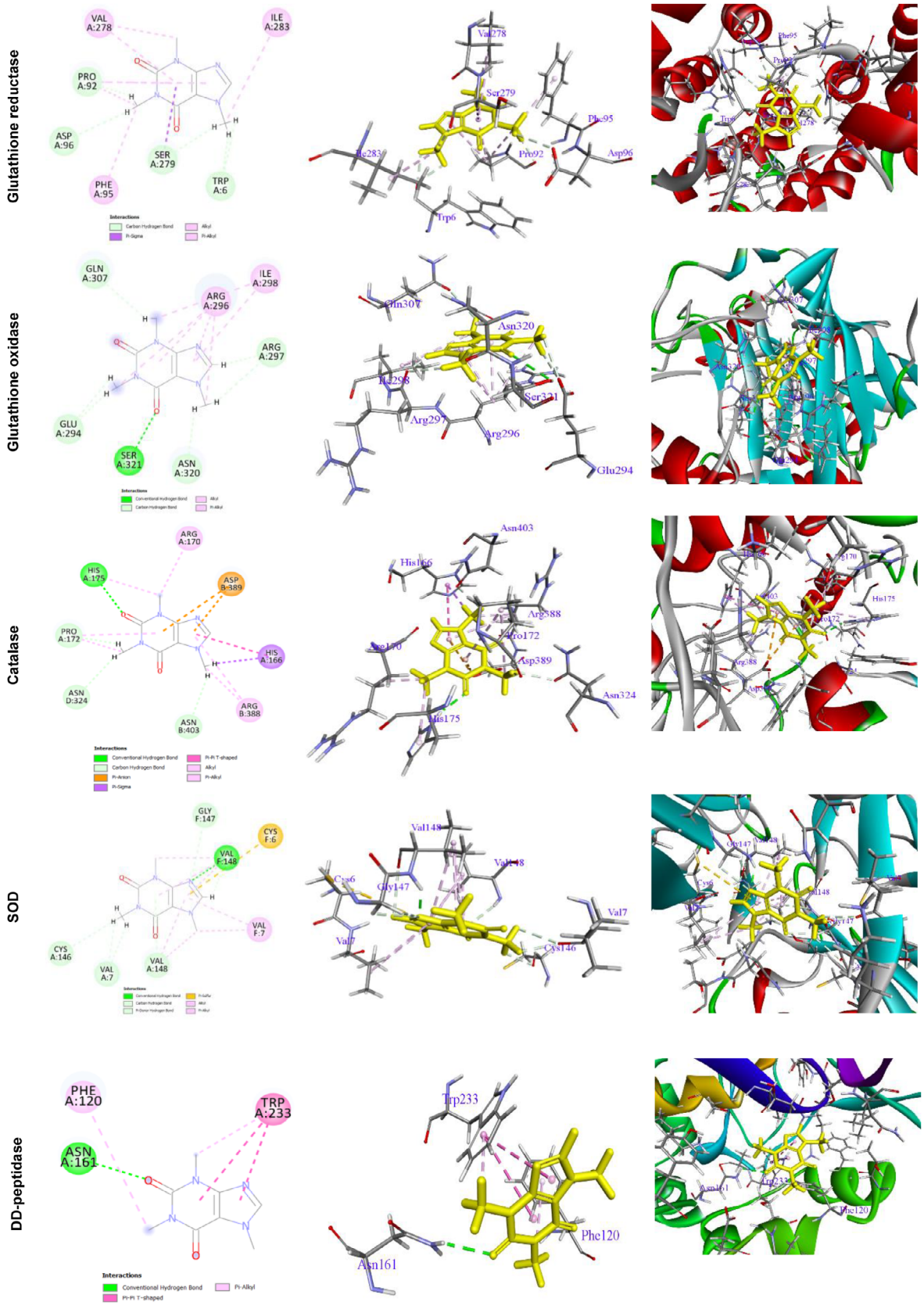

FIGURE 5 | Interaction of caffeine with glutathione reductase, glutathione oxidase, catalase, SOD, and DD-peptidase, (a) 2D, (b) general, and (c) 3D images.

compound X, an oxyferryl derivative without a radical site. To complete the catalytic cycle, this other structure must be reduced to iron-containing catalase. However, most one-electron donor molecules of catalase do not react with compound X, that is, they do not restore the native enzyme. Compound x does not participate in the catalytic cycle with hydrogen peroxide, and its accumulation can therefore lead to inhibition of catalase activity [54].

Caffeine, which is found in plants, is the most suitable psychostimulant for enhancing motor activation, altering mood, facilitating information processing, and improving cognitive and motor performance. Studies have shown that caffeine and its metabolites have an antioxidant effect [55]. Several studies suggest that long-term caffeine intake may increase the activity of antioxidant enzymes in the liver and heart, thereby reducing the risk of developing neurodegenerative diseases [56]. In some cases, chronic ingestion of caffeine can lead to increased activity of antioxidant enzymes, which indicates a possible neuroprotective role. As the biochemical mechanism underlying caffeine's effects is believed to involve the blockade of adenosine receptors, the altered activities of antioxidant enzymes suggest that caffeine affects receptor function [57]. In this study, in silico studies confirm that caffeine can inhibit antioxidant enzymes. These findings highlight how the formation of smaller and more reactive molecules through pyrolysis such as caffeine and palmitic acid derivatives, enhances the antioxidant and antibacterial performance of the products, thereby reinforcing the mechanistic link between molecular interactions and the observed biological outcomes.

3 | Conclusions

In our study, we determined the chemical profile and characteristic properties of the methanol–chloroform extract, pyrolysis product, and AgNPs obtained from CSS fruit. The phytochemical contents of the extract and pyrolysis product were analyzed using spectrophotometric methods such as LC–ESI–MS/MS, GC–MS/MS, and NMR. At the same time, the characteristic properties of AgNPs were assessed using spectrophotometric techniques like TEM, XRD, FE-SEM, FE-SEM–EDX, FT-IR, and UV–Vis. The antioxidant (DPPH$^{\cdot}$ and FRAP) and phenolic contents (FCR) of the obtained extract and pyrolysis product were investigated through the innovative use of a potentiometric biosensor method. Interestingly, the pyrolysis product was found to be more effective than the extract in terms of antioxidant activity. It was also observed that pyrolysis exhibited a higher inhibitory effect against diabetic enzymes (α-amylase and α-glucosidase). In addition, the antibacterial activities of extracts, pyrolysis, and AgNP samples against Gram-negative and Gram-positive bacteria were examined, revealing that both AgNPs and pyrolysis exhibited strong antibacterial activity. This suggests that pyrolysis converts complex organic substances into simpler molecules through thermal decomposition in an oxygen-free environment, thereby enhancing their activity. NMR analysis of the pyrolysis liquid indicates that the absence of a double bond likely results from biological activities (antioxidant and antibacterial), facilitating the molecule's rapid penetration into bacterial cell walls.

Furthermore, this lighter molecule may enhance activity by aiding the entry of other molecules into the bacterial cell wall. Molecular docking studies exploring the interactions between caffeine, the main component of the pyrolysis product, and antioxidant enzymes (glutathione reductase, glutathione oxidase, catalase, SOD) and an antibacterial enzyme (DD- peptidase) showed that caffeine exhibits high binding energies of −4.7, −6.3, −6.9, −4.7, and −4.8 kcal/mol with SOD, catalase, glutathione reductase, glutathione oxidase, and DD-peptidase, respectively. Thus, the large amounts of waste generated daily in agriculture, industry, and forestry present significant environmental challenges and cannot be easily converted into value-added products. By employing environmentally friendly pyrolysis, bio-oils can be obtained from plant materials that are otherwise not suitable for thermal processing, thereby increasing their use as antioxidants, antibiotics, antifungals, and insecticides. This potential will likely expand the application of pyrolysis products in the food, cosmetics, and industrial sectors, with future studies shedding further light on these prospects.

The chemical profile and characteristic properties of the methanol–chloroform extract, the pyrolysis product, and the AgNPs obtained from CSS fruit were determined. For a more comprehensive understanding of the bioactive composition of CSS, it is also recommended that a comparative analysis of the volatile compounds that could be obtained through supercritical CO_2 extraction be included. This advanced extraction technique is well known for its ability to isolate thermolabile and low molecular weight volatile constituents without degradation. Comparing these supercritical CO_2-derived volatiles with those present in the solvent extract and pyrolysis product would be expected to provide deeper insight into how extraction conditions influence the chemical composition and potential biological activity of the resulting fractions.

4 | Experimental Section

4.1 | Plant Materials

CSS fruit was collected on August 22, 2023 in Iğdır University Agricultural Research Center, Aralık district of Iğdır Province in Türkiye. The species identification was made by Prof. Dr. Ahmet Zafer Tel and stored in the herbarium (INWM00000248) of Igdir University.

4.2 | Extraction Methods

Extraction for phytochemical analysis and biological activity: The caper fruit samples were taken to the laboratory, where they were crushed and dried. Having been thoroughly dried in a cool, airy environment, the samples were ground into a powder using a grinder. A 50 g sample was transferred to a 750 mL Erlenmeyer flask. Extraction was first carried out with hexane over the course of a week to obtain volatile oils and fatty acids, and this process was repeated three times. Then, extraction was carried out using a 1:1 methanol–chloroform solvent mixture under the same conditions. The solvent mixture was evaporated using a rotary evaporator. The samples were stored at +4°C for further analysis.

4.3 | Synthesis of AgNPs

The methanol–chloroform (1:1) extract from CSS fruits was used to biosynthesize AgNPs. First, the fruits were thoroughly washed in cold water, dried in an oven at 30°C, and then crushed using a mechanical shredder. A 20 g extract of dry fruits was extracted with 150 mL of water for 15 min [58]. The aqueous extract was then filtered through Whatman No. 1 filter paper. About 80 mL of the extract was transferred to an Erlenmeyer flask and stirred at room temperature using a magnetic stirrer set at 600 rpm. A 10 mM $AgNO_3$ solution was added to the extract, and the mixture was stirred to facilitate the formation of AgNPs. A color change in the solution indicated the formation after approximately 12 h. Subsequently, the AgNP-containing solution was centrifuged at 10 000 rpm for 20 min. The precipitates obtained after centrifugation were washed twice with ethyl alcohol and deionized water to remove impurities. They were then dried in a low-temperature oven for further characterization and analysis.

4.4 | Pyrolysis Application

The pyrolysis process of the ground caper sample was carried out with a fixed-bed pyrolysis device (reactor) in an inert nitrogen atmosphere. In the pyrolysis study, a 100 g solid sample was placed in the feed reactor pool. It was then exposed to the nitrogen gas at 300°C for about 2 h in an inert environment at a heating rate of 10°C/min. Then the liquid sample in the collection container was filled into airtight bottles (Figure 1) [59].

4.5 | Characterization of AgNPs

Synthesized AgNPs were characterized by TEM, XRD, FE-SEM, FE-SEM–EDX, and UV–Vis spectrophotometry (Agilent Cary 60). In green synthesis research, UV–Vis spectroscopy is generally the preferred analytical method for identifying organic molecules, ions, or more complex structures, with wavelength ranges spanning the ultraviolet and visible light spectrum. It was used to examine the absorption spectrum of AgNPs in the 400–800 nm wavelength range. FT-IR spectroscopy (Agilent Cary 630) is the preferred characterization method for identifying functional groups in molecular structures. This method was used to reveal changes in the formation of AgNPs nanoparticles, such as the disappearance of the strong vibrational bands at 1610 and 1390 cm^{-1}, the broad vibrational band at 3384 cm^{-1}, and the vibrational band at 1375 cm^{-1} due to the closing effect of the (C—O) group. FE-SEM (ZEISS GeminiSEM) was used to analyze the morphological changes (oval or spherical) on the surface, the energy distribution, and the presence of elemental silver. TEM analysis was performed to determine the size and shape of the nanoparticles (square, rectangular, hemispherical, and spherical). XRD was used to characterize the produced nanoparticles. This technique confirms the silver content of the particles and provides information about their structure [60, 61].

4.6 | Phenolic Content Analysis by LC–ESI–MS/MS

The content analysis of the extract and the pyrolysis sample was performed with the Agilent 1260 Infinity II LC–ESI–MS/MS instrument. An Agilent Poroshell120 EC-C18 reversed-phase analytical column (100 mm × 3.0 mm, 2.7 μm) was used for chromatographic separation. Instrument conditions: the mobile phase consisted of a mixture of formic acid (0.1%) and ammonium formate (5.0 mM) in water (Phase A) and a mixture of formic acid (0.1%) and ammonium formate (5.0 mM) in methanol (Phase B). The gradient program was set as follows: 20% B for 1–5 min, 55% B for 6–15 min, 85% B for 16–25 min, and 5% B for 25–30 min. The injection volume was 5.12 μL, with a flow rate of 0.40 mL/min. The capillary voltage was set to 4000 V, and the column temperature was set to 40°C. For the analysis, the plant extract and the pyrolysis sample (50 mg each) were dissolved in methanol (1.0 mL) in an Eppendorf tube. Then hexane was added, after which the mixture was centrifuged at 10 000 rpm for five minutes. The methanol phase (100 μL) was diluted by the addition of water (450 μL) and an equal volume of methanol (450 μL). After filtration using a 0.22 μm filter, the solution was injected into the device. Thirty-nine standard compounds (Figure S4) were used in the analysis [62, 63].

4.7 | Fatty Acid Content Analysis by GC–MS/MS

The fatty acid content of caper extract and pyrolysis liquid was analyzed by Agilent 7000 A GC/MS Triple Quad GC–MS/MS. Analyses were performed using an Agilent HP-5 (5%-phenyl)-methylpolysiloxane column (30 m × 0.25 mm × 0.25 μm). The initial temperature was set at 50°C and held for 2 min. It was then increased to 140°C at a rate of 3°C/min, followed by an increase to 220°C at a rate of 4°C/min for 10 min. The temperature was then held at 4°C/min until reaching 270°C. The sample was then held at 270°C for a further 30 min. The ion temperature of the MS detector was set to 280°C. After filtering the sample using a 0.22 μm disposable syringe filter, it was run with a flow rate of 1 mL/min of He gas and an injection volume of 1 μL at a ratio of 1:10. A 30 mg sample was dissolved in 2 mL of methanol, to which 2 mL of *n*-hexane was then added. One milliliter of 1 M KOH solution was then added, after which the mixture was vortexed at 2500 rpm for 30 s. The upper phase (the *n*-hexane phase), which contained the fatty acid methyl esters, was removed and filtered through a 0.22 μm PVDF filter before being injected [64].

4.8 | NMR Spectroscopy

Caper extract and pyrolysis product were dissolved in $CDCl_3$. Its structure was determined by Bruker- 400 MHz ^1H NMR.

4.9 | FCR (Total Phenolic) Test

The total amount of caper extract and pyrolysis product was determined by FCR-SPMB. In this study, the antioxidant capacity of the samples was evaluated by measuring the total amount of phenolic compounds. This method is based on measuring the amount of FCR, which remains unchanged despite the presence of antioxidants. For spectrometer measurements, the test results are given as GA equivalent (mg/g extract). In our study, we evaluated our results as the equivalent amount of GA. For this purpose, a GA-FCR calibration diagram was constructed

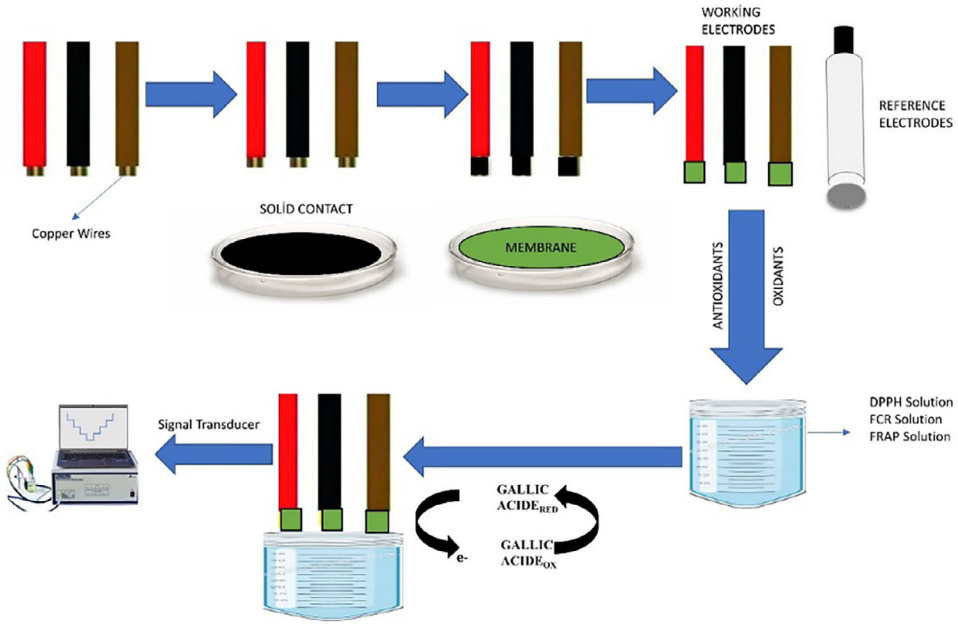

FIGURE 6 | Schematic of the determination of antioxidant activity by potentiometric biosensor method.

to determine the GA equivalent, which is the amount of FCR reduced by the antioxidant species in the environment [65].

4.10 | DPPH$^{\cdot}$ Scavenging Activity Test

In this study, DPPH$^{\cdot}$ scavenging activity was evaluated by measuring DPPH$^{\cdot}$ that was not quenched in the environment by the interaction of antioxidant species. Ten milliliters of the plant extract was taken, and 10 mL of a 100 µg/mL DPPH$^{\cdot}$ solution was added. It was waited for 30 min until the interaction reaction of the antioxidant species in the plant content with DPPH$^{\cdot}$ was completed, and the potential values were measured by directly immersing these samples in DPPH-SPMB. The following formula was used. The results were expressed as percentages [65].

$$\%\text{RSA} = \frac{[(E_1 - E_0) - (E_2 - E_0)]}{E_1 - E_0} \times 100$$

where E_0 is the potential value of the plant sample, E_1 is the potential value of the DPPH$^{\cdot}$ standard solution, and E_2 is the potential value of the DPPH$^{\cdot}$ scavenging activity remaining in the medium after 30 min of reaction.

4.11 | FRAP Iron(III) Reducing Activity Test

The activity of Fe(III) ions in a dissolved environment was successfully measured using FRAP-selective PVC membrane biosensors (FRAP-SPMB) (Figure 6). In our study, iron(III) reduction activity was evaluated by measuring the amount of Fe(III) ion that remained unreduced in the environment as a result of the reduction of Fe(III) to Fe(II) by antioxidant species. The results of Fe(III) reduction activity in spectrometer measurements are expressed as trolox equivalent (mg/g extract). Therefore, in our study, we reported our results as Trolox equivalent. For this purpose, a calibration curve for Fe(III)-equivalent Trolox was created. Using this calibration curve, the Fe(III) reduction activity of the plant extracts was determined potentiometrically [65].

4.12 | Enzyme Inhibitions

4.12.1 | XO Inhibition

Fifty microliters of sample or allopurinol solution, 100 µL of 0.041 mM xanthine, and 50 µL of freshly prepared 0.1 U/mL XO in phosphate buffer (pH 7.5) were added to the 96-well microplate. The mixture was incubated at 37°C for 5 min. The reaction was then stopped by adding 100 µL of 1 M HCl. The absorbance was measured using a 292 nm UV/VIS spectrophotometer [66]. IC_{50} (µg/mL) values were calculated using the absorbance values.

4.12.2 | α-Amylase Inhibition

α-Amylase inhibition of samples was determined using the iodine–potassium iodide (KI) method [67]. In a 96-well plate, 82 µL of samples or acarbose at different concentrations, 10 µL of 1 U α-amylase (in 20 mM pH 6.9 potassium phosphate buffer) were mixed homogeneously and kept at 37°C for 10 min. The mixture was mixed homogeneously with 8 µL of 1% starch solution and incubated at 37°C for 12 min. The mixture was added to 50 µL of 10% HCl and 15 µL of iodine–KI (2.5 mM iodine + 6.5 mM KI) and mixed homogeneously. The samples were kept in boiling water for 10 min. The absorbance values of each mixture were measured at 620 nm using a BIOTEK (Epoch2) microplate reader, and the results were determined by calculating the IC_{50} (µg/mL) values.

4.12.3 | α-Glucosidase Inhibition

α-Glucosidase inhibition of samples was determined using the PNPG (4-*p*-nitrophenyl α-D-glucopyranoside) method [68]. Ten

microliters of different concentrations of samples or acarbose, 25 µL of 0.2 U α-glucosidase (in 20 mM pH 6.9 potassium phosphate buffer) were mixed homogeneously in a 96-well plate. The mixture was homogeneously mixed with 25 µL of 0.5 mM PNPG and 20 µL of 20 mM pH 6.9 potassium phosphate buffer. The samples were kept at 37°C for 12 min. The mixture was mixed homogeneously in 100 µL of 0.2 M Na_2CO_3. The absorbance values of each mixture were measured at 410 nm using a BIOTEK (Epoch2) microplate reader and the results were determined by calculating the IC_{50} (µg/mL) values.

4.12.4 | Antimicrobial Assay by the Disc Diffusion Method

The disc diffusion method was used to determine the antibacterial activities of caper, nanoparticle, pyrolysis, and extract samples [69]. In the antimicrobial activity studies, the concentrations of bacteria were adjusted to 10^8 CFU/mL 0.5 McFarland. Three gram-negative (*E. coli*, *K. pneumoniae*, and *P. aeruginosa*) and one gram-positive (*S. aureus*) bacterial strain were selected for the study. The antibiotics used were gentamicin (10 µg), amoxicillin (25 µg), and tetracycline (30 µg). For the test strains, 6 mm blank discs (BIOANALYSE Blank Disc in Cartridge ASD10011) were used. The strain concentrations were set at 80, 40, 20, and 10 mg/mL. After the bacteria were applied to the media using the spreading technique, the discs impregnated with the extract were placed in Petri dishes. They were incubated at 37°C for 16–24 h. At the end of the incubation, the zones formed around the discs were measured in mm.

4.13 | Molecular Docking Studies

In the molecular docking studies, the molecular structure of caffeine was first drawn in ChemDraw, and the minimum energy was calculated using Chem3D program. The molecular structure was saved in mol2 format. The enzymes that used the 3D protein crystal structure of our tests, such as glutathione reductase [PDB ID: 1AXN], glutathione oxidase [PDB ID: 1GPI], catalase [PDB ID: 1QQW], superoxide dismutase [PDB ID: 2C9V], and DD-peptidase [PDB ID: 3PTE] were selected from the RSCB Protein Data Bank (PDB). The program MVD (Molegro Virtual Docker) was used to determine the interaction of the molecule with the active site of the enzyme. All data were integrated to observe the 2D and 3D interaction of the molecules with the active site of the enzyme using the Discovery Studio program [70, 71].

4.14 | Statistical Analysis

Triplicate in vitro antioxidant activities and standard deviation values were calculated. The IBM SPSS 20.0 program was used. One-way ANOVA, Tukey HSD, and multiple comparison tests were applied to all data obtained. The statistical significance level of the data was expressed as $p < 0.05$.

Author Contributions

Semiha Yenigün: software, investigation, methodology, validation, visualization, writing – original draft, and writing – review and editing. **Yunus Basar**: conceptualization, data curation, formal analysis, investigation, methodology, software, validation, visualization, writing – original draft, and writing – review and editing. **Ibrahim Demirtas**: conceptualization, data curation, formal analysis, funding acquisition, investigation, methodology, supervision, validation, visualization, writing – original draft, and writing – review and editing. **Tevfik Ozen**: investigation, methodology, validation, visualization, and writing – review and editing. **Büşran Sunyar**: investigation, methodology, validation, visualization. **Aybek Yiğit**: conceptualization, data curation, investigation, methodology, validation, visualization, writing – original draft. **İlyas Yıldız**: methodology, validation, conceptualization, data curation, formal analysis. **Mehmet Hakkı Alma**: conceptualization, data curation, funding acquisition, investigation, methodology, resources, supervision, writing – review and editing.

Acknowledgments

The authors would like to thank TÜBA (Turkish Academy of Sciences) for Pyrolysis and Iğdır University for the financial support provided for the production of value-added raw materials from agricultural products (Project no. YİP0723İ01).

Conflicts of Interest

The authors declare no conflicts of interest.

Data Availability Statement

The data that support the findings of this study are available in the Supporting Information of this article.

References

1. M. A. Demirci, Y. Ipek, F. Gul, T. Ozen, and I. Demirtas, "Extraction, Isolation of Heat-Resistance Phenolic Compounds, Antioxidant Properties, Characterization and Purification of 5-Hydroxymaltol From Turkish Apple Pulps," *Food Chemistry* 269 (2018): 111–117, https://doi.org/10.1016/j.foodchem.2018.06.147.

2. X. Tan, P. Chen, L. Xiao, et al., "Extraction, Purification, Structural Characterization, and Anti-Inflammatory Activity of a Polysaccharide From *Lespedeza formosa*," *International Journal of Biological Macromolecules* 300 (2025): 140154, https://doi.org/10.1016/j.ijbiomac.2025.140154.

3. F. Hassan, C. Liu, M. Mehboob, et al., "Potential of Dietary Hemp and Cannabinoids to Modulate Immune Response to Enhance Health and Performance in Animals: Opportunities and Challenges," *Frontiers in Immunology* 14 (2023): 1285052, https://doi.org/10.3389/fimmu.2023.1285052.

4. M. B. Salem, H. Affes, K. Ksouda, et al., "Pharmacological Studies of Artichoke Leaf Extract and Their Health Benefits," *Plant Foods for Human Nutrition* 70, no. 4 (2015): 441–453, https://doi.org/10.1007/s11130-015-0503-8.

5. S. Shi, K. Li, J. Peng, et al., "Chemical Characterization of Extracts of Leaves of *Kadsua coccinea* (Lem.) A.C. Sm. by UHPLC-Q-Exactive Orbitrap Mass Spectrometry and Assessment of Their Antioxidant and Anti-Inflammatory Activities," *Biomedicine & Pharmacotherapy* 149 (2022): 112828, https://doi.org/10.1016/j.biopha.2022.112828.

6. S. Koldaş, I. Demirtas, T. Ozen, M. A. Demirci, and L. Behçet, "Phytochemical Screening, Anticancer and Antioxidant Activities of *Origanum vulgare* L. ssp. Viride (Boiss.) Hayek, a Plant of Traditional Usage," *Journal of the Science of Food and Agriculture* 95, no. 4 (2015): 786–798, https://doi.org/10.1002/jsfa.6903.

7. A. V. Bridgwater, *Progress in Thermochemical Biomass Conversion* (John Wiley & Sons, 2008).

8. M. Ertaş and M. Hakkı Alma, "Pyrolysis of Laurel (*Laurus nobilis* L.) Extraction Residues in a Fixed-bed Reactor: Characterization of Bio-Oil

and Bio-Char," *Journal of Analytical and Applied Pyrolysis* 88, no. 1 (2010): 22–29, https://doi.org/10.1016/j.jaap.2010.02.006.

9. C. Mattos, M. C. C. Veloso, G. A. Romeiro, and E. Folly, "Biocidal Applications Trends of Bio-Oils From Pyrolysis: Characterization of Several Conditions and Biomass, A Review," *Journal of Analytical and Applied Pyrolysis* 139 (2019): 1–12, https://doi.org/10.1016/j.jaap.2018.12.029.

10. E. Duman and M. M. Özcan, "Physicochemical Properties of Seeds of Capparis Species Growing Wild in Turkey," *Environmental Monitoring and Assessment* 186, no. 4 (2014): 2393–2398, https://doi.org/10.1007/s10661-013-3546-z.

11. T. Gull, F. Anwar, B. Sultana, M. A. C. Alcayde, and W. Nouman, "*Capparis* Species: A Potential Source of Bioactives and High-Value Components: A Review," *Industrial Crops and Products* 67 (2015): 81–96, https://doi.org/10.1016/j.indcrop.2014.12.059.

12. H. Uslu, D. Erdağ, G. Atila, et al., "Investigation of Antifungal and Antioxidant Properties of *Capparis ovata* Methanolic Extracts," *Mehmet Akif Ersoy University Journal of Health Sciences Institute* 6, no. 2 (2018): 60–66, https://doi.org/10.24998/maeusabed.460081.

13. R. Muhaidat, M. Al-Qudah, A. Al-shayeb, et al., "Chemical Profile and Antibacterial Activity of Crude Fractions and Essential Oils of *Capparis ovata* Desf. and *Capparis spinosa* L. (Capparaceae)," *International Journal of Integrative Biology* 14 (2013): 39–47.

14. M. Rafique, I. Sadaf, M. S. Rafique, and M. B. Tahir, "A Review on Green Synthesis of Silver Nanoparticles and Their Applications," *Artificial Cells, Nanomedicine, and Biotechnology* 45, no. 7 (2017): 1272–1291, https://doi.org/10.1080/21691401.2016.1241792.

15. R. S. Varma, "Greener Approach to Nanomaterials and Their Sustainable Applications," *Current Opinion in Chemical Engineering* 1, no. 2 (2012): 123–128, https://doi.org/10.1016/j.coche.2011.12.002.

16. N. Ahmad, "Green Synthesis of Silver Nanoparticles Using Extracts of *Ananas comosus*," *Green and Sustainable Chemistry* 2 (2012) 141–147, https://doi.org/10.4236/gsc.2012.24020.

17. M. Kowshik, N. Deshmukh, W. Vogel, J. Urban, S. K. Kulkarni, and K. M. Paknikar, "Microbial Synthesis of Semiconductor CdS Nanoparticles, Their Characterization, and Their Use in the Fabrication of an Ideal Diode," *Biotechnology and Bioengineering* 78, no. 5 (2002): 583–588, https://doi.org/10.1002/bit.10233.

18. Anshup, J. S. Venkataraman, C. Subramaniam, et al., "Growth of Gold Nanoparticles in Human Cells," *Langmuir* 21, no. 25 (2005): 11562–11567, https://doi.org/10.1021/la0519249.

19. K. Govindaraju, S. K. Basha, V. G. Kumar, and G. Singaravelu, "Silver, Gold and Bimetallic Nanoparticles Production Using Single-Cell Protein (*Spirulina platensis*) Geitler," *Journal of Materials Science* 43 (2008): 5115–5122, https://doi.org/10.1007/s10853-008-2745-4.

20. A. Królikowska, A. Kudelski, A. Michota, and J. Bukowska, "SERS Studies on the Structure of Thioglycolic Acid Monolayers on Silver and Gold," *Surface Science* 532–535 (2003): 227–232, https://doi.org/10.1016/S0039-6028(03)00094-3.

21. A. Kumar, S. Mandal, P. R. Selvakannan, R. Pasricha, A. B. Mandale, and M. Sastry, "Investigation Into the Interaction Between Surface-Bound Alkylamines and Gold Nanoparticles," *Langmuir* 19, no. 15 (2003): 6277–6282, https://doi.org/10.1021/la034209c.

22. S. Yaping, N. Atorngitjawat, and M. Meziani, "Preparation of Silver Nanoparticles via Rapid Expansion of Water in Carbon Dioxide Microemulsion Into Reductant Solution," *Langmuir* 17 (2001): 5707–5710, https://doi.org/10.1021/la0103057.

23. A. M. Abu-Dief, L. H. Abdel-Rahman, M. A. Abd-El Sayed, M. M. Zikry, and A. Nafady, "Green Synthesis of AgNPs() Ultilizing *Delonix regia* Extract as Anticancer and Antimicrobial Agents**," *ChemistrySelect* 5 (2020): 13263–13268, https://doi.org/10.1002/slct.202003218.

24. M. Cakić, S. Glišić, D. Cvetković, et al., "Green Synthesis, Characterization and Antimicrobial Activity of Silver Nanoparticles Produced From *Fumaria officinalis* L. Plant Extract," *Colloid Journal* 80 (2018): 803–813, https://doi.org/10.1134/S1061933X18070013.

25. M. Nilavukkarasi, S. Vijayakumar, and S. Prathip Kumar, "Biological Synthesis and Characterization of Silver Nanoparticles With *Capparis zeylanica* L. Leaf Extract for Potent Antimicrobial and Anti Proliferation Efficiency," *Materials Science for Energy Technologies* 3 (2020): 371–376, https://doi.org/10.1016/j.mset.2020.02.008.

26. S. Iravani, "Green Synthesis of Metal Nanoparticles Using Plants," *Green Chemistry* 13, no. 10 (2011): 2638, https://doi.org/10.1039/C1GC15386B.

27. V. K. Vidhu, S. A. Aromal, and D. Philip, "Green Synthesis of Silver Nanoparticles Using *Macrotyloma uniflorum*," *Spectrochimica Acta Part A: Molecular and Biomolecular Spectroscopy* 83, no. 1 (2011): 392–397, https://doi.org/10.1016/j.saa.2011.08.051.

28. P. Suresh, A. Doss, R. P. Praveen Pole, and M. Devika, "Green Synthesis, Characterization and Antioxidant Activity of Bimetallic (Ag-ZnO) Nanoparticles Using *Capparis zeylanica* Leaf Extract," *Biomass Conversion and Biorefinery* 14 (2023): 16451–16459, https://doi.org/10.1007/s13399-023-03743-7.

29. P. Rauwel, S. Küünal, S. Ferdov, and E. Rauwel, "A Review on the Green Synthesis of Silver Nanoparticles and Their Morphologies Studied via TEM," *Advances in Materials Science and Engineering* 2015 (2015): 682749, https://doi.org/10.1155/2015/682749.

30. Y. Başar, S. Yenigün, M. H. Alma, İ. Demirtas, and T. Ozen, "Characterization of Silver Nanoparticles by Green Synthesis Method Using Pedalium murex Leaf Extract and Their Antibacterial Activity," *Applied Nanoscience* 6 (2015): 399–408, https://doi.org/10.1007/s13204-015-0449-z.

31. B. Ajitha, Y. Ashok Kumar Reddy, and P. S. Reddy, "Biogenic Nano-Scale Silver Particles by *Tephrosia purpurea* Leaf Extract and Their Inborn Antimicrobial Activity," *Spectrochimica Acta Part A: Molecular and Biomolecular Spectroscopy* 121 (2014): 164–172, https://doi.org/10.1016/j.saa.2013.10.077.

32. M. Marrelli, M. P. Argentieri, P. Avato, F. Menichini, and F. Conforti, "Inhibitory Effect on Lipid Absorption and Variability of Chemical Constituents From *Capparis sicula* subsp. *sicula* and *Capparis orientalis*," *Chemistry & Biodiversity* 13, no. 6 (2016): 755–761, https://doi.org/10.1002/cbdv.201500240.

33. Ö. Isildak, I. Yildiz, and N. Genc, "A New Potentiometric PVC Membrane Sensor for the Determination of DPPH Radical Scavenging Activity of Plant Extracts," *Food Chemistry* 373, no. Pt A (2022): 131420, https://doi.org/10.1016/j.foodchem.2021.131420.

34. Ö. Isildak, I. Yildiz, N. Genç, D. Sabanci, and I. Işildak, "New Potentiometric PVC Membrane Electrode for Ferric Reduction Antioxidant Power Assay," *Food Chemistry* 423 (2023): 136261, https://doi.org/10.1016/j.foodchem.2023.136261.

35. Y. Başar, S. Yenigün, M. H. Alma, İ. Demirtas, and T. Ozen, "Fruit Extracts of *Rosa canina* L. and *Rosa pimpinellifolia* L.: Phytochemical Profiles, In Vitro Antioxidant, Anti-Inflammatory, Xanthine Oxidase Inhibitory Effects, and In Silico Molecular Dynamics Studies," *KSU Journal of Agriculture and Nature* 28, no. 3 (2025): 636–649, https://doi.org/10.18016/ksutarimdoga.vi.1639294.

36. S. A. Antar, N. A. Ashour, M. Sharaky, et al., "Diabetes Mellitus: Classification, Mediators, and Complications; a Gate to Identify Potential Targets for the Development of New Effective Treatments," *Biomedicine & Pharmacotherapy* 168 (2023): 115734, https://doi.org/10.1016/j.biopha.2023.115734.

37. S. Tannous, T. Stellbrinck, A. Hoter, and H. Y. Naim, "Interaction Between the α-Glucosidases, Sucrase-Isomaltase and Maltase-Glucoamylase, in Human Intestinal Brush Border Membranes and Its Potential Impact on Disaccharide Digestion," *Frontiers in Molecular Biosciences* 10 (2023): 1160860, https://doi.org/10.3389/fmolb.2023.1160860.

38. M. Roney, A. K. M. M. Huq, K. Rullah, N. B. Zamri, and M. F. F. Mohd Aluwi, "Curcumin, a Bioactive Compound of Turmeric (*Curcuma longa*) and Its Derivatives as α-Amylase and α-Glucosidase Inhibitors,"

Cell Biochemistry and Biophysics 83, no. 1 (2025): 53–71, https://doi.org/10.1007/s12013-024-01477-5.

39. E. D. Cavassin, L. F. P. De Figueiredo, J. P. Otoch, et al., "Comparison of Methods to Detect the In Vitro Activity of Silver Nanoparticles (AgNP) Against Multidrug Resistant Bacteria," *Journal of Nanobiotechnology* 13 (2015): 64, https://doi.org/10.1186/s12951-015-0120-6.

40. T. Bruna, F. Maldonado-Bravo, P. Jara, and N. Caro, "Silver Nanoparticles and Their Antibacterial Applications," *International Journal of Molecular Sciences* 22, no. 13 (2021): 7202, https://doi.org/10.3390/ijms22137202.

41. Y. Qing, L. Cheng, R. Li, et al., "Potential Antibacterial Mechanism of Silver Nanoparticles and the Optimization of Orthopedic Implants by Advanced Modification Technologies," *International Journal of Nanomedicine* 13 (2018): 3311–3327, https://doi.org/10.2147/ijn.S165125.

42. X. Luo, X. Xie, Y. Meng, T. Sun, J. Ding, and W. Zhou, "Ligands Dissociation Induced Gold Nanoparticles Aggregation for Colorimetric Al^{3+} Detection," *Analytica Chimica Acta* 1087 (2019): 76–85, https://doi.org/10.1016/j.aca.2019.08.045.

43. P. Wu, R. Huang, C. Chen, et al., "Aptamer-AuNP-Conjugated Carboxymethyl Chitosan–Functionalized Graphene Oxide for Colorimetric Identification of *Salmonella typhimurium*," *Microchimica Acta* 189, no. 11 (2022): 408, https://doi.org/10.1007/s00604-022-05494-0.

44. M. Seong and D. G. Lee, "Silver Nanoparticles Against *Salmonella enterica* Serotype Typhimurium: Role of Inner Membrane Dysfunction," *Current Microbiology* 74, no. 6 (2017): 661–670, https://doi.org/10.1007/s00284-017-1235-9.

45. E. Z. Gomaa, "Silver Nanoparticles as an Antimicrobial Agent: A Case Study on *Staphylococcus aureus* and *Escherichia coli* as Models for Gram-Positive and Gram-Negative Bacteria," *Journal of General and Applied Microbiology* 63, no. 1 (2017): 36–43, https://doi.org/10.2323/jgam.2016.07.004.

46. D. Savoia, "Plant-Derived Antimicrobial Compounds: Alternatives to Antibiotics," *Future Microbiology* 7, no. 8 (2012): 979–990, https://doi.org/10.2217/fmb.12.68.

47. M. M. Cowan, "Plant Products as Antimicrobial Agents," *Clinical Microbiology Reviews* 12, no. 4 (1999): 564–582, https://doi.org/10.1128/cmr.12.4.564.

48. F. Benakashani, A. R. Allafchian, and S. A. H. Jalali, "Biosynthesis of Silver Nanoparticles Using *Capparis spinosa* L. Leaf Extract and Their Antibacterial Activity," *Karbala International Journal of Modern Science* 2, no. 4 (2016): 251–258, https://doi.org/10.1016/j.kijoms.2016.08.004.

49. E. Javadian, A. Biabangard, M. Ghafari, S. Saeidi, and B. Fazeli-Nasab, "Green Synthesis of Silver Nanoparticles and Antibacterial Properties of Extracts of *Capparis spinosa* Leaves," *Journal of Medicinal Plants & By-Products* 13, no. 2 (2024): 329–343, https://doi.org/10.22034/jmpb.2023.361363.1528.

50. S. H. Salmen, E. Damra, T. A. Alahmadi, and S. A. Alharbi, "Green Synthesis, Characterization and Antibacterial Activity of Silver Nanoparticles From *Capparis spinosa* Leaf Extract," *Revista de Chimie* 72 (2021): 145–152, https://doi.org/10.37358/RC.21.1.8411.

51. A. B. Lansdown, "Silver I: Its Antibacterial Properties and Mechanism of Action," *Journal of Wound Care* 11, no. 4 (2002): 125–130, https://doi.org/10.12968/jowc.2002.11.4.26389.

52. L. Pinzi and G. Rastelli, "Molecular Docking: Shifting Paradigms in Drug Discovery," *International Journal of Molecular Sciences* 20, no. 18 (2019): 4331, https://doi.org/10.3390/ijms20184331.

53. H. Alonso, A. A. Bliznyuk, and J. E. Gready, "Combining Docking and Molecular Dynamic Simulations in Drug Design," *Medicinal Research Reviews* 26, no. 5 (2006): 531–568, https://doi.org/10.1002/med.20067.

54. H. Sepasi Tehrani and A. A. Moosavi-Movahedi, "Catalase and Its Mysteries," *Progress in Biophysics and Molecular Biology* 140 (2018): 5–12, https://doi.org/10.1016/j.pbiomolbio.2018.03.001.

55. J. Krych and L. Gebicka, "Catalase Is Inhibited by Flavonoids," *International Journal of Biological Macromolecules* 58 (2013): 148–153, https://doi.org/10.1016/j.ijbiomac.2013.03.070.

56. C. Lee, "Antioxidant Ability of Caffeine and Its Metabolites Based on the Study of Oxygen Radical Absorbing Capacity and Inhibition of LDL Peroxidation," *Clinica Chimica Acta* 295, no. 1–2 (2000): 141–154, https://doi.org/10.1016/s0009-8981(00)00201-1.

57. A. Kalda, L. Yu, E. Oztas, and J.-F. Chen, "Novel Neuroprotection by Caffeine and Adenosine A2A Receptor Antagonists in Animal Models of Parkinson's Disease," *Journal of the Neurological Sciences* 248, no. 1–2 (2006): 9–15, https://doi.org/10.1016/j.jns.2006.05.003.

58. C. G. Noschang, R. Krolow, L. F. Pettenuzzo, et al., "Interactions Between Chronic Stress and Chronic Consumption of Caffeine on the Enzymatic Antioxidant System," *Neurochemical Research* 34, no. 9 (2009): 1568–1574, https://doi.org/10.1007/s11064-009-9945-4.

59. B. Ajitha, Y. A. Reddy, and P. Reddy, "Biogenic Nano-Scale Silver Particles by *Tephrosia purpurea* Leaf Extract and Their Inborn Antimicrobial Activity," *Spectrochimica Acta Part A: Molecular and Biomolecular Spectroscopy* 121C (2013): 164–172, https://doi.org/10.1016/j.saa.2013.10.077.

60. Y. Başar, M. S. Nas, M. H. Alma, İ. Demirtaş, and M. H. Çalımlı, "Chemical Structure and Characterization of Bio-Oils Isolated From Walnut Shells by Different Processes," Journal of Scientific Reports-A no. 57 (2024): 144–152, https://doi.org/10.59313/jsr-a.1433854.

61. Y. Başar, A. Yiğit, A. Karacalı Tunç, and B. M. Sarıtaş, "Lavandula Stoechas Extract; Synthesis of Silver Nanoparticles (Nature-Friendly Green Synthesis Method), Characterization, Antimicrobial Activity and In Silico Molecular Docking Study," *Current Perspectives on Medicinal and Aromatic Plants* 7, no. 1 (2024): 24–33, https://doi.org/10.38093/cupmap.1461976.

62. M. H. Çalımlı, Y. Başar, F. Gül, M. S. Nas, and M. H. Alma, "Investigation of Value-Added Compounds Derived From Oak Wood Using Hydrothermal Processing Techniques and Comprehensive Analytical Approaches (HPLC, GC-MS, FT-IR, and NMR)," *International Journal of Chemistry and Technology* 8, no. 1 (2024): 51–59, https://doi.org/10.32571/ijct.1365592.

63. I. Yildiz, Y. Başar, R. Erenler, M. H. Alma, and M. H. Calimli, "A Phytochemical Content Analysis, and Antioxidant Activity Evaluation Using a Novel Method on *Melilotus officinalis* Flower," *South African Journal of Botany* 174 (2024): 686–693, https://doi.org/10.1016/j.sajb.2024.09.060.

64. R. Erenler, I. Yıldız, E. N. Geçer, et al., "Phytochemical Analyses of *Ebenus haussknechtii* Flowers: Quantification of Phenolics, Antioxidants Effect, and Molecular Docking Studies," *Journal of Integrative and Anatolian Medicine* 5, no. 2 (2024): 1–9, https://doi.org/10.53445/batd.1479874.

65. Y. Başar, F. Gül, M. Karadağ, M. H. Alma, İ. Demirtas, and A. Z. Tel, "Determination of the Volatile, Phenolic and Fatty Acid Contents of *Helichrysum plicatum* by Chromatographic Methods," *Turkish Journal of Biodiversity* 7, no. 2 (2024): 83–94, https://doi.org/10.38059/biodiversity.1600406.

66. Ö. Isildak, I. Yildiz, N. Genç, D. Sabanci, and I. Işildak, "New Potentiometric PVC Membrane Electrode for Ferric Reduction Antioxidant Power Assay," *Food Chemistry* 423 (2023): 136261, https://doi.org/10.1016/j.foodchem.2023.136261.

67. Z. Li, W. Zhang, M. A. Abubaker, Q. Shu, and Y. Liu, "In Silico Identification and Experimental Validation of Two Types of Angiotensin-Converting Enzyme (ACE) and Xanthine Oxidase (XO) Milk Inhibitory Peptides," *Food Chemistry* 464 (2025): 141864, https://doi.org/10.1016/j.foodchem.2024.141864.

68. P. Ercan and S. N. El, "Inhibitory Effects of Chickpea and *Tribulus terrestris* on Lipase, α-Amylase and α-Glucosidase," *Food Chemistry* 205 (2016): 163–169, https://doi.org/10.1016/j.foodchem.2016.03.012.

69. S. Sancheti, S. Sancheti, and S.-Y. Seo, "Evaluation of Antiglycosidase and Anticholinesterase Activities of *Boehmeria nivea*," *Pakistan Journal of Pharmaceutical Sciences* 23, no. 2 (2010): 236–240.

70. J. Hudzicki, *Kirby-Bauer Disk Diffusion Susceptibility Test Protocol* (American Society for Microbiology, 2009).

71. G. F. Chi, S. Khan, Y. Başar, et al., "Antibacterial Flavonoids From *Tetrapleura tetraptera* (Fabaceae) Fruit Pulp, In Silico Studies," *South African Journal of Botany* 180 (2025): 96–106, https://doi.org/10.1016/j.sajb.2025.02.026.

72. M. Gok, Y. Basar, S. Yenigun, et al., "Bioactive Apigenin-7-O-β-Glucoside and Rosmarinic Acid Molecules from Two *Nepeta* Species: Bioactivity-Guided Isolation, In Vitro Evaluations, Pharmacokinetic and In Silico Approaches as Metabolic Enzyme Inhibition Agents," *Phytochemical Analysis* (2025): 1677–1694, https://doi.org/10.1002/pca.3536.

Supporting Information

Additional supporting information can be found online in the Supporting Information section.

Supporting File 1: cbdv70851-sup-0001-SuppMat.pdf